ADVANCED MATERIALS TECHNOLOGIES
www.advmattechnol.de

Green Fabrication of Stackable Laser-Induced Graphene Micro-Supercapacitors under Ambient Conditions: Toward the Design of Truly Sustainable Technological Platforms

Sara L. Silvestre, Maria Morais, Raquel R. A. Soares, Zachary T. Johnson, Eric Benson, Elisabeth Ainsley, Veronica Pham, Jonathan C. Claussen, Carmen L. Gomes, Rodrigo Martins, Elvira Fortunato, Luis Pereira, and João Coelho**

Extensive research into green technologies is driven by the worldwide push for eco-friendly materials and energy solutions. The focus is on synergies that prioritize sustainability and environmental benefits. This study explores the potential of abundant, non-toxic, and sustainable resources such as paper, lignin-enriched paper, and cork for producing laser-induced graphene (LIG) supercapacitor electrodes with improved capacitance. A single-step methodology using a CO_2 laser system is developed for fabricating these electrodes under ambient conditions, providing an environmentally friendly alternative to conventional carbon sources. The resulting green micro-supercapacitors (MSCs) achieve impressive areal capacitance (≈7–10 mF cm^{-2}) and power and energy densities (≈4 μW cm^{-2} and ≈0.77 µWh cm^{-2} at 0.01 mA cm^{-2}). Stability tests conducted over 5000 charge–discharge cycles demonstrate a capacitance retention of ≈80–85%, highlighting the device durability. These LIG-based devices offer versatility, allowing voltage output adjustment through stacked and sandwich MSCs configurations (parallel or series), suitable for various large-scale applications. This study demonstrates that it is possible to create high-quality energy storage devices based on biodegradable materials. This development can lead to progress in renewable energy and off-grid technology, as well as a reduction in electronic waste.

1. Introduction

Sustainability is now the driving force for a greener and more technologically advanced future, in line with the global goals set out by the United Nations 2030 Agenda.[1] Therefore, to facilitate the transition to a sustainable world and to meet the increasing demand to reduce global dependence on fossil fuels and electronic waste (e-waste), it has become crucial to explore the potential of abundant and renewable materials.[2–4] Among the natural materials available, cellulose, and lignocellulosic by-products are noteworthy, as they are biodegradable and hold promise for the development of green electronics.[2,5] In addition to their environmental benefits, these materials offer several advantages over traditional polymer substrates, including cost effectiveness, ease of handling, and improved customization for a wide range of electronic applications, including disposable wearable

S. L. Silvestre, M. Morais, R. Martins, E. Fortunato, L. Pereira, J. Coelho
CENIMAT
i3N
Department of Materials Science
School of Science and Technology
NOVA University Lisbon and CEMOP/UNINOVA
Caparica Portugal
E-mail: si.silvestre@campus.fct.unl.pt; jmesquita@us.es

The ORCID identification number(s) for the author(s) of this article can be found under https://doi.org/10.1002/admt.202400261

DOI: 10.1002/admt.202400261

R. R. A. Soares, Z. T. Johnson, J. C. Claussen, C. L. Gomes
Department of Mechanical Engineering
Iowa State University
Ames, IA 50011, USA

E. Benson, E. Ainsley, V. Pham
School of Art + Design
Graphic Design Program
University of Illinois Urbana-Champaign
Champaign, IL 61820, USA

J. Coelho
Dpto. Física de la Materia Condensada
Universidad de Sevilla
Avda. Reina Mercedes S/N, Sevilla 41012, Spain

J. Coelho
Instituto de Ciencia de Materiales de Sevilla (Universidad de Sevilla-CSIC)
Avda. Americo Vespucio 49, Sevilla 41092, Spain

electronics, paper-based circuits, and packaging solutions.[6] However, not all cellulose-based electronics are straightforward in terms of complexity.[7] For example, paper-based electronics typically involve complex processes such as inkjet-based deposition, lithography, and spray coating, among others.[8] While these approaches enable the creation of innovative electronic functionalities on sustainable substrates, they still raise concerns in terms of complexity, limited design flexibility, and time required to manufacture specific devices.[9] The application of laser technology has proven to be an impressive solution to overcome these challenges, offering a simpler, faster, and more controlled methodology.[10] This cost-effective approach not only enables the large-scale conversion of natural, abundant, and renewable resources into green laser-induced graphene (gLIG) structures with ease, but it also offers environmental advantages over conventional LIG fabricated on commercial materials such as polyimide.[10–12] In addition, gLIG fulfills essential and desired electrode requirements – high electrical conductivity and surface area. This property is primarily due to the inherent nature of the substrates, which results in a highly porous structure with a substantial surface area.[11] Furthermore, the high defect density in the structure of gLIG can enhance its electroactivity and catalytic potential for various electrochemical applications.[13] Therefore, the promising properties of gLIG have led to its use in a variety of fields, including the fabrication of biosensors,[14–16] supercapacitors,[17–22] humidity and temperature sensors,[23] mechanical sensors,[24,25] among others. When designing sustainable platforms, there is a need for a stable and continuous power supply for various functions, including sensing, data communication, and signal conditioning.[7] Therefore, researchers have explored micro-supercapacitors as an effective and reliable energy storage solution.[26] MSCs have the potential to meet these requirements and withstand adverse conditions, especially where conventional power sources are limited. They offer several advantages over other storage devices, such as high-power density, fast charging and discharging, and long cycle life.[27,28] Various gLIG-MSCs have been developed on different substrates such as paper, leaves, lignin, wood, cork, and others, demonstrating different ranges of specific capacitance and overall electrochemical performance.[11,13] Although LIG fabrication is a straightforward method, it often results in materials with different morphologies and properties, making device and substrate comparison a cumbersome process.[11] In this work, gLIG is fabricated using a CO_2 laser under ambient conditions and is assembled into sandwich-shaped micro-supercapacitors. First, the laser writing process is optimized on different substrates (paper, lignin-enriched paper, and cork) to obtain LIG with high electrical conductivity and the highest quality. This optimization is controlled through Raman spectroscopy by mapping and studying the characteristic graphitic peaks. This research is characterized by the exploration sustainable and abundant substrates while also investigating the contribution of lignin substrates to improve LIG production. Following this, MSCs are assembled to understand the influence of LIG properties derived from the different substrates on the electrochemical performance of the devices. This study also demonstrates a novel ability to interconnect individual MSC units in both series and parallel configurations. This distinctive adaptability significantly increases the overall capacity of the system, enabling tailor-made applications. In addition, an environmentally conscious approach to energy has been introduced with the development of green LIG MSCs. These assembled devices have also demonstrated their effectiveness by successfully powering electronic devices, such as a watch integrated with a humidity and temperature sensor. This demonstration highlights the high potential and practical utility of the devices fabricated, positioning our work as a pioneering contribution in the field of LIG-based energy storage platforms.

2. Results and Discussion

2.1. LIG Fabrication and Characterization

Laser conversion for the production of gLIG using various renewable materials has been extensively studied, using bio-based carbon sources and substrates such as wood, leaves, cork, husks, and cellulose.[11] This work aims to investigate and compare the conversion of three cellulosic substrates: paper, lignin-enriched paper, and cork. In particular, lignin-enriched paper is a variant produced by environmentally friendly industries that emphasize the incorporation of lignin content – often considered a by-product and waste – into recycled substrates or related by-products. Higher lignin content in substrates has been shown to be beneficial in producing higher quality LIG with more desirable Raman profiles, characterized by lower defect density in the graphitic structures formed.[11] This ensures a better carbon hybridization yield during laser conversion, which directly improves the conductive properties of the LIG, as discussed below.[29]

Recognizing the importance of selecting the most appropriate precursor for each target application, this research thoroughly investigates the tunning of LIG production from these substrates, thus providing the flexibility to tune the LIG electrode properties and architecture.

Due to the highly flammable nature of the materials used, the substrates were impregnated with a borax fire retardant solution prior to laser exposure, followed by a drying process. This measure is intended to protect the substrate from thermal degradation and prevent undesirable effects such as substrate ablation and the formation of fragile LIG structures. Similar issues have previously been observed in studies with other cellulosic substrates.[14,21] Furthermore, the borax pre-treatment is a critical step in the process, mainly because these natural substrates are converted into LIG in a non-inert atmosphere.[11] Some reports show that the use of boric acid in substrate pretreatment can lead to a boron doping effect during electrode fabrication.[30–32] As far as we are concerned, sodium tetraborate was not used as a doping agent, but rather as a fire retardant for the formation of LIG on these highly sensitive substrates. It cannot be excluded that some boron doping takes place on the prepared samples. However, in our case it is not possible to compare the LIG properties on a treated substrate with those on untreated samples. Therefore, the extent and significance of boron on the prepared LIG cannot be properly assessed and further characterization was not pursued.

After impregnating the substrates with a flame-retardant to fine-tune the LIG properties, different laser conditions such as the laser defocus, power, and speed were investigated,

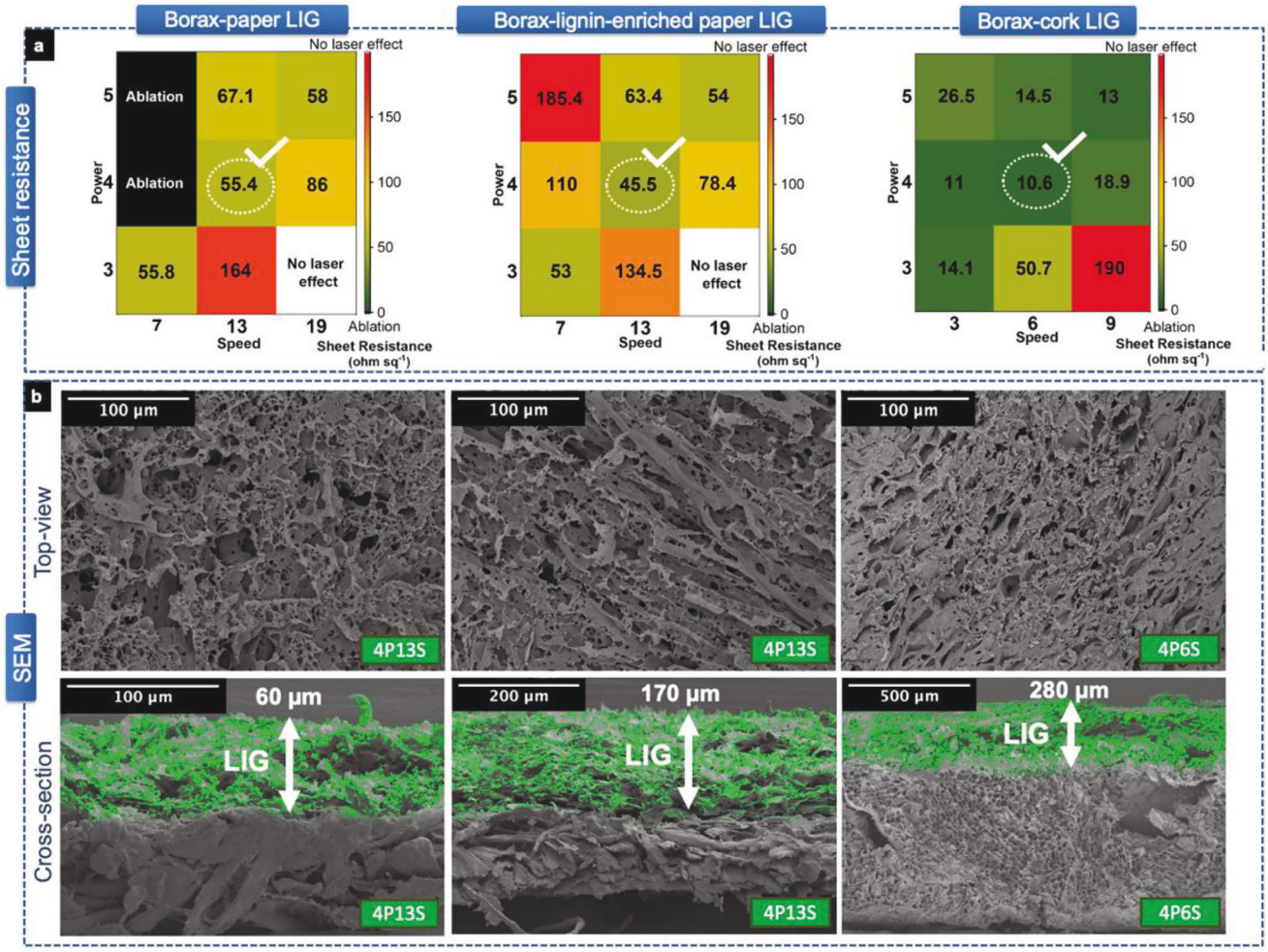

Figure 1. a) Matrix of sheet resistance values for different laser settings (in percentage) and b) SEM (Scanning electron microscopy) images of the top-view and cross-section (green highlighted) of the borax-paper (BP), borax-lignin-enriched paper (BLEP), and borax-cork (BC) laser-induced graphene fabricated using the optimal laser settings (identified on the bottom right corner) corresponding to the lowest sheet resistance.

demonstrating the importance of precise laser settings to achieve distinct LIG properties, which have a direct impact on the electrochemical performance of LIG-based MSCs.[33,34] By first optimizing the defocus, a foundation was laid for the subsequent adjustments to power and speed, as the study of defocus conditions helped to initiate the optimization process and minimize potential issues of overheating and substrate damage. For example, adjusting the defocus distance from the focal point leads to changes in the energy distribution over the area undergoing LIG conversion, which affects the substrate carbonization rate and LIG formation, homogeneity, thickness, porosity, conductivity, crystallinity, among other factors.[11,35,36] Therefore, a laser beam position of 2 mm below the focal point was set as the optimum parameter for all substrates. This setting results in the lowest sheet resistance, as shown in Figure S1 (Supporting Information). This property has previously been highlighted as one of the most important aspects to be improved when fine-tuning of LIG electrode fabrication to meet the electrical conductivity criteria for desired electronic applications. The defocus distance was consistently maintained throughout the subsequent work, proving to be an effective strategy to avoid simultaneous changes in multiple parameters.

Continuing the evaluation of the LIG from different substrates, the analysis was extended to assess their morphology and surface topology. **Figure** 1a shows a comprehensive analysis of the correlation between the variations in power and speed applied during laser irradiation and the resulting changes in LIG sheet resistance values for all substrates.

This matrix shows not only the sheet resistance values but also discloses the influence of the laser parameters on the electrical properties of each substrate. The matrix values are expressed as percentages, considering the maximum power and grating speed of the CO_2 laser system are 75 W and 3.05 m s^{-1}, respectively.

In addition to the matrix of sheet resistance values, Figure 1b complements the analysis by showing top view and cross-sectional SEM images of the three different LIG substrates produced at optimal laser settings. The scale has been adjusted to match the dimensions of the samples, with the aim of achieving higher resolution in the cross-sectional images. These images provide valuable morphological information on the surface

topography, layering, and thickness of the LIG. This morphological information can be used to correlate the LIG microstructure with its conductivity.

The observed reduction in sheet resistance values, traced along the diagonal of each matrix, is consistent with existing literature.[14,17,21] For the paper and lignin-enriched paper substrates, the optimal conditions were obtained at a laser power of 4% and a speed of 13% (3 W @ 0.40 m s^{-1}) resulting in sheet resistances of 55.4 ± 2.8 ohm sq^{-1} (for paper) and 45.5 ± 2.3 ohm sq^{-1} (for lignin-enriched paper), respectively. Similarly, for the cork substrate, the optimal LIG electrode formation was achieved at a laser power of 4% and a speed of 6% (3 W @ 0.18 m s^{-1}), yielding a sheet resistance of 10.6 ± 0.5 ohm sq^{-1}. Notably, a higher degree of graphitization of the substrates with higher lignin content was observed. A comparison of paper and lignin-enriched paper with cork reveals that cork exhibits greater tolerance and thermal resistance to laser irradiation, thereby preserving its structural integrity even at lower processing speeds. This is due to the fact that paper substrates are more susceptible to rapid heating and combustion during laser irradiation due to their higher thermal conductivity compared to cork. As previously reported, the thermal conductivity values for cellulose paper and cork are ≈0.076 and 0.045 W m^{-1} K^{-1}, respectively.[37,38] This fact highlights the importance of the substrate composition and its inherent characteristics before laser conversion, which are determinants for the successful formation of conductive LIG. It is noteworthy that the sheet resistance values of cork's are significantly lower than those of paper and lignin-enriched paper while maintaining the integrity of the underlying substrate. Despite flame-retardant pre-treatment, the susceptibility of sensitive substrates to ablation is a common phenomenon.[14,21] Nevertheless, this issue can be effectively addressed by applying higher processing speeds, and in this study, a speed two times higher for paper and lignin-enriched paper than the cork substrate was employed. This approach minimized the potential ablative effect on these substrates while still enabling the production of LIG with good electrical properties.[11,28] Additionally, sheet resistance can also be influenced by the morphology of the LIG obtained. As evidenced by existing literature,[10,39,40] it is well-established that the morphological structure of LIG can directly affect its electrical conductivity. Therefore, Figure 1b presents surface and cross-sectional views of the LIG samples produced from the different substrates, which yielded the lowest and optimal sheet resistance values. The images show a uniformly interconnected and porous LIG network for all substrates, which plays a pivotal role in the efficient charge transport within its framework. When examining the relationship between LIG's thickness and its sheet resistance, it can be observed that thicker LIG derived from cork exhibits a distinctive advantage in terms of electrical conductivity compared to LIG derived from paper and lignin-enriched paper. This characteristic may appear contradictory because thicker films usually exhibit lower conductivity when compared to thinner layers. Thinner layers offer a higher density of conductive pathways within the LIG matrix, often leading to improved conductivity.[10] Nevertheless, when thicker LIG possesses a well-connected network of conductive pathways, it can facilitate the formation of an increased abundance of graphene layers. Consequently, this offers a multitude of routes for charge carriers to move within its structure, ultimately promoting higher electrical conductivity.

To further understand the properties and potential applications of the fabricated LIG, the samples were studied by Raman spectroscopy. As depicted in **Figure 2**, the obtained spectra suggest the successful formation of LIG on paper, lignin-enriched paper, and cork substrates.

In Figure 2a, Raman mapping provides insights into the structural variations of LIG produced on these natural substrates along their surface. The I_{2D}/I_G and I_D/I_G ratios were evaluated by tracking the characteristic graphitic peaks measured at different locations on the samples and by assessing their intercorrelation. In Figure 2b, the peaks show the formation of LIG in all samples with characteristic Raman peaks identified. These include peaks D (≈1350 cm^{-1}), G (≈1580 cm^{-1}), and 2D (≈2700 cm^{-1}).[11,13] The color variations observed in each mapping result from increased or decreased peak intensity, which provides valuable information about the material's composition and quality.

Lower I_D/I_G ratios indicate the presence of higher-quality graphene domains with a lower density of defects in the formed graphitic structures.[29] This characteristic is prominently observed on lignin-enriched paper and cork substrates, where the D peak intensity is notably reduced. In contrast, when using a pure paper substrate, a prevalence of the D peak over the G peak is observed, indicative of a higher density of defects, and consequently, lower-quality LIG. The phenomenon of reduced D peak intensity has been reported for substrates with higher lignin content, resulting in an increased degree of graphitization. This consistent with the decreasing trend in sheet resistance, which follows the order: BP-LIG (≈55.4 ohm sq^{-1}), BLEP-LIG (≈45.5 ohm sq^{-1}), and BC-LIG (≈10.6 ohm sq^{-1}).[41] Upon correlation with SEM images, borax-cork LIG appears to be thicker than paper-based LIG and exhibits a more uniform and interconnected lattice structure. Consequently, cork-based LIG exhibits a lower sheet resistance than paper-based LIG.

Conversely, the presence of the 2D peak indicates the formation of graphitic material, and the I_{2D}/I_G ratios are often used as criteria to identify the number of graphene layers.[11,42] Therefore, the higher intensity of 2D peaks identified in paper-based LIG compared to cork-LIG, along with higher I_{2D}/I_G ratios, is mainly attributed to fewer graphene layers in the material.

To support the results above, X-ray photoelectron spectroscopy (XPS) characterization was conducted, which showed the distinct presence of graphene structures.[11,17,21] This confirmation is derived from an analysis of the high-resolution spectrum of the C 1s in all samples (Figure S2, Supporting Information).[11]

2.2. MSCs Fabrication and Stack Assembly

The fabrication process for the single-device MSCs is visually illustrated in **Figure 3**. This process involved three distinct steps: a) electrode fabrication via laser-inducing technique, subsequent b) deposition of the electrolyte, and the final c) assembly of the components into functional MSCs. The solid PVA/H_2SO_4 electrolyte was carefully deposited onto the LIG electrodes through a drop-casting technique (Figure 3b). Next, a vacuum process was employed for 10 min. This additional step was designed to promote increased electrolyte penetration into the LIG structure, enhancing the contact area between the electrolyte and electrode. A

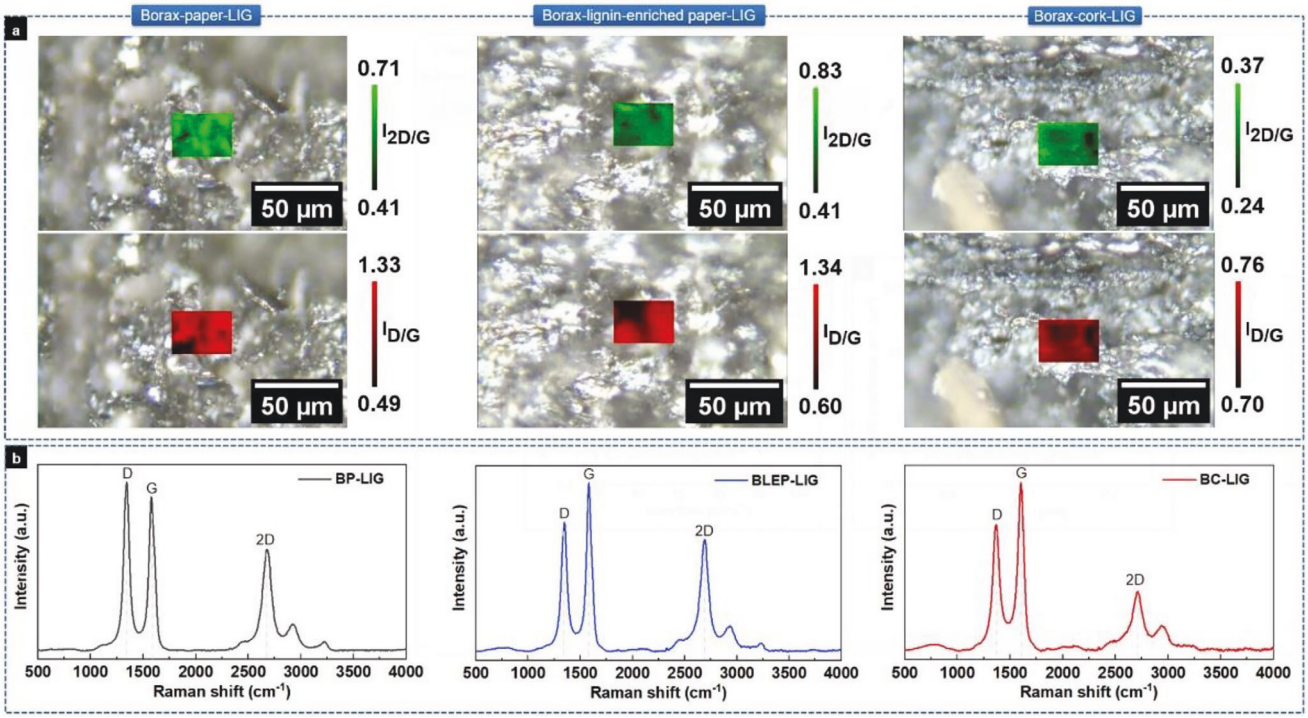

Figure 2. Raman a) mapping and b) spectra of borax-paper, borax-lignin-enriched paper, and borax-cork LIG.

paper separator was employed to prevent device short-circuiting problems and retain the electrolyte within the desired area.

The adoption of the sandwich configuration over the interdigitated one was intended to fulfill the energy-related targets set forth for systems that require enhanced energy and power density, efficient electrode-electrolyte interaction, and integration in compact formats.

For multiple connected LIG electrodes, a single-step patterning approach of multiple electrodes was initially considered. However, this approach has drawbacks, including limited independence from each individually fabricated MSC and potential short-circuit issues. An alternative strategy emerged: patterning distinct electrodes separately to create single MSCs and then assembling them one by one. This method allows for the integration of the desired number of MSCs, achieved by gently connecting each unit through their silver pads, as seen in **Figure 4**. This strategy enhances the control over the final energy storage device as it enables individual replacement of MSC, the addition or removal of units for specific application needs, adaptability across diverse applications, and reusability. Integration of

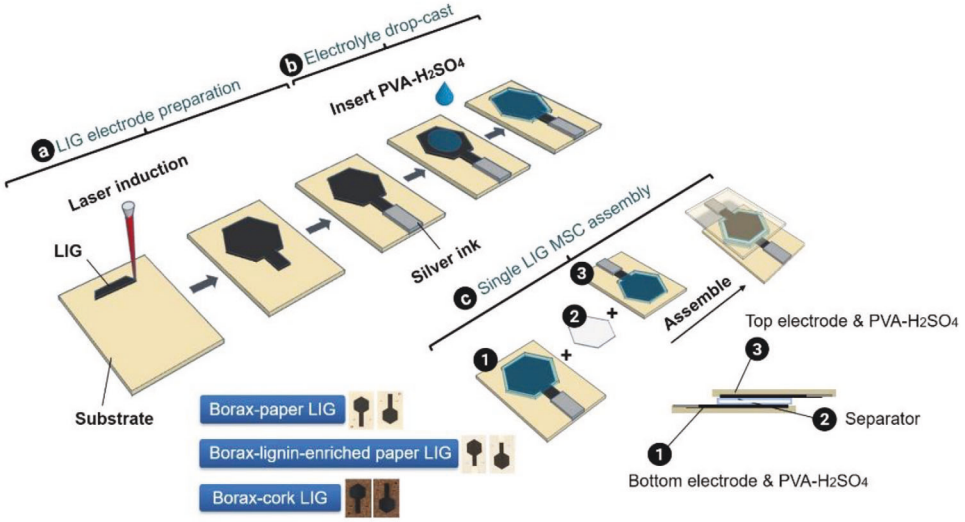

Figure 3. Schematic illustration of a single LIG-MSC fabrication from a) electrode preparation, b) electrolyte deposition, and c) device assembly.

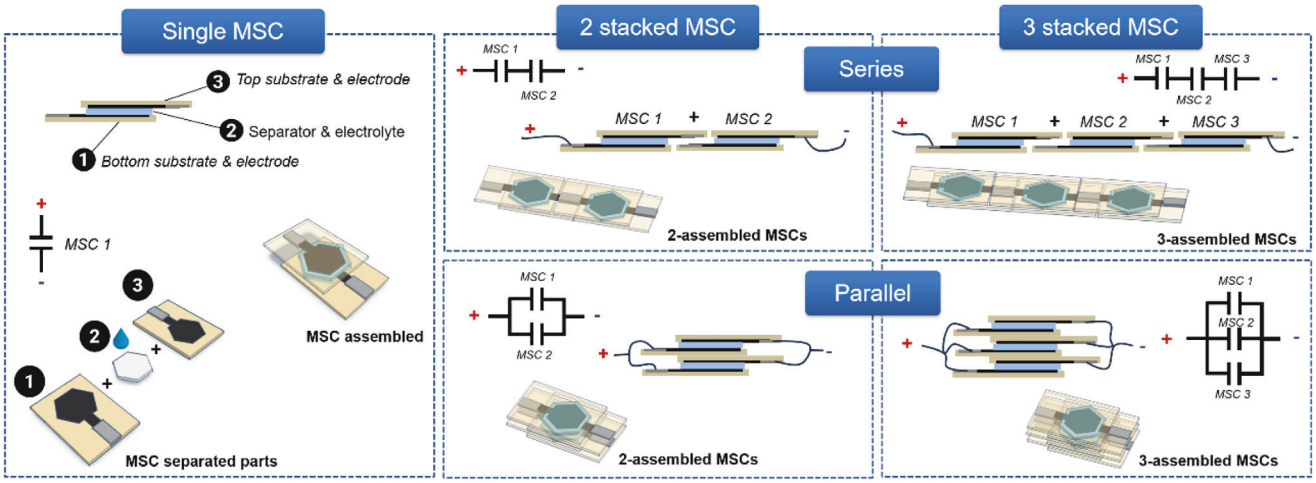

Figure 4. Illustration of single MSC alongside stacked MSCs in both series and parallel arrangements.

stacked MSCs offers significant benefits to the energy storage system, including increased energy and power density, enhanced total capacitance, improved energy efficiency, and customization flexibility.[43,44] Consequently, this strategy was subjected to exploration and is depicted in Figure 4, which presents single MSC and stacked MSCs arrangements arranged in series and parallel configurations, thereby demonstrating the reliability of the assemblies for compact energy storage solutions.

The subsequent section presents a comparative analysis of the electrochemical performance of various configurations and the number of employed MSC units. It highlights the stacked configuration's capability to meet diverse energy storage requirements.

2.3. Electrochemical Performance of Sandwich Supercapacitors

A comprehensive assessment of the sustainable MSCs was conducted to explore their energy storage and delivery capabilities. This evaluation involved the examination of cyclic voltammetry (CV) and galvanostatic charge–discharge (GCD) analyses performed across all devices. In **Figure** 5a,b, illustrates the presence of leaf-like shaped CV curves for MSCs derived from BP and BLEP. In contrast the BC MSC (Figure 5c) exhibits a quasi-rectangular shape, which is indicative of the typical electrical double layer (EDL) capacitive behavior.[45]

Figure 5a-c illustrates the impact of varying scan rates on the diffusion of ions within the electrode. At lower scan rates, ions have more time to diffuse and penetrate the deeper pores of the electrode, leading to enhanced areal capacitance. As the scan rate increases from 5 to 100 mV s^{-1}, the distinct leaf-like shaped CV curves become more pronounced due to constrained ion diffusion. This is typically observed when the available time for ion diffusion is reduced at higher scan rates.[27] The BC MSCs benefit from the inherent substrate characteristics, including greater porosity, increased LIG thickness, and a larger surface area.[18] These attributes contribute to maintaining quasi-rectangular CV curves even at higher scan rates, which highlights the cork electrode's capability to withstand more challenging conditions. This resilience is crucial for applications requiring rapid charge and discharge cycles.

The GCD graphs demonstrate near-symmetrical triangular curves across all devices, in accordance with the typical EDL behavior observed in the CV analysis. The observed asymmetry in the LIG-derived MSCs' charge and discharge times can be attributed to ion kinetics within the porous electrode structure. This is influenced by electrochemical reactions occurring at the electrode-electrolyte interface.[17] Factors such as porosity, thickness, and the presence of surface functional groups within the electrode matrix contribute to variations in ion transport rates.[11,13] Despite the observed variations, all devices exhibit relatively similar behavior, suggesting that the overall electrochemical performance remains consistent across all devices.

Figure 6a presents a summary of the calculated areal capacitance values of all devices as the current density increases from 0.01 to 0.2 mA cm^{-2}, as extracted from the curves.

At a current density of 0.01 mA cm^{-2}, the highest capacitance of 7.34 mF cm^{-2} was achieved for BP MSC, 9.51 mF cm^{-2} for BLEP MSC, and 8.65 mF cm^{-2} for BC MSC.

Table 1 compares the performances of gLIG and polyimide-based LIG MSCs, in addition to the values obtained from this study. The inclusion criteria considered a range of factors, including electrode designs, laser types, substrate type, optimized laser conditions, and those with the highest relevance and closest similarity to the presented study.

The capacitances of the best-performing devices in this work, when compared with those reported in the literature, suggest reliability in the obtained results. This contributes to a growing body of knowledge around gLIG as a promising alternative for energy storage devices.

In this study, the sandwich configuration was selected over the interdigitated, primarily due to the objective of prioritizing a larger effective surface area for the electrode-electrolyte interface, following reports that demonstrated improved capacitance.[18]

While certain applications may prioritize high packing density, often favored by interdigitated designs, others may prioritize a greater effective surface area, favored by a sandwich

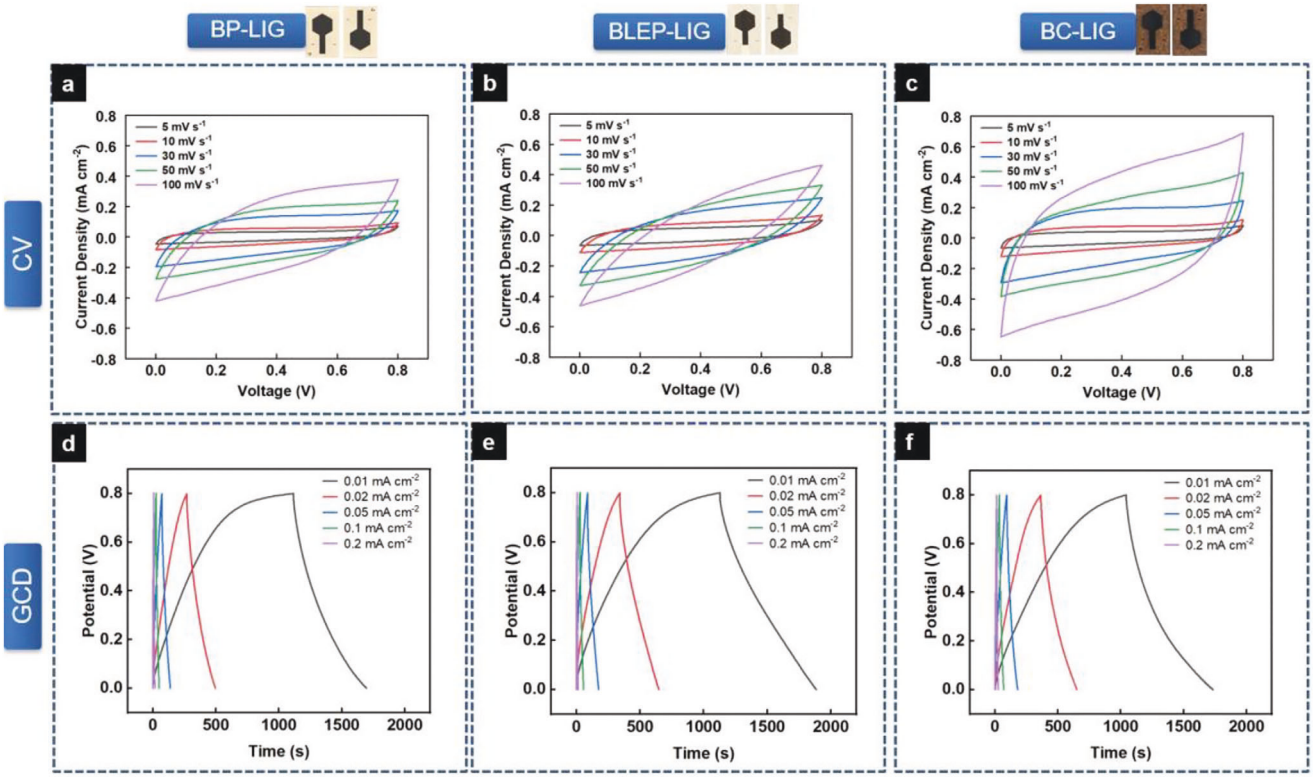

Figure 5. Cyclic voltammograms of a) BP, b) BLEP, and c) BC based LIG MSCs; respectively, and corresponding galvanostatic charge and discharge curves on (d–f).

configuration. Nevertheless, exploring the most suitable configuration requires a careful balance of multiple factors, including electrode thickness, electrolyte used, ion diffusion paths, application-specific needs, among others.[27,45] These considerations are essential for optimizing the overall performance and efficiency of the supercapacitor system.

Furthermore, this study aimed to assess the suitability and versatility of renewable materials in the practical development of MSC. All devices showed relatively similar electrochemical performances (Figure 6). However, under higher current densities, BC MSC consistently demonstrated superior performance. This resilient behavior suggests a notable capacity to sustain performance under increased current densities, making it particularly intriguing and promising candidate for applications that demand stable electrochemical performance.

The Ragone plots in Figure 6b confirm the high-energy and high-power density achieved for all devices. At a current density of 0.01 mA cm^{-2}, the highest energy density (E_A) values were 0.73, 0.85, and 0.77 μWh cm^{-2} for BP, BLEP, and BC MSCs, respectively. At the same current value, the power density (P_A) was able to reach 4 μW cm^{-2} for all substrates.

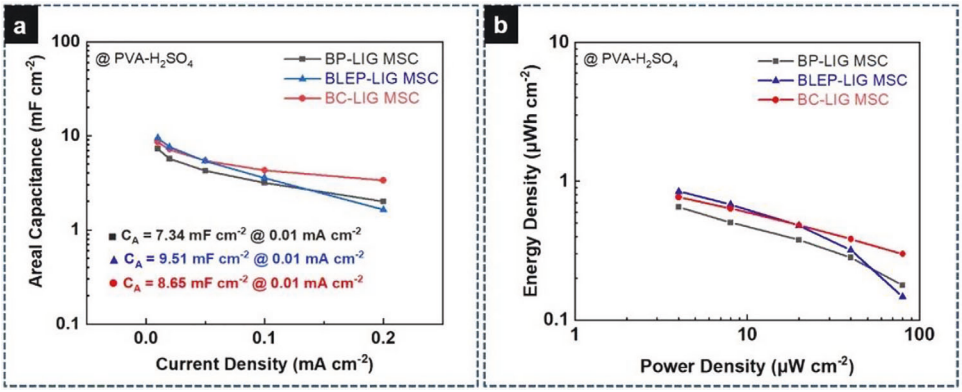

Figure 6. a) Areal capacitance (C_A) from GCD analysis and b) ragone plot of all devices.

Table 1. Comparison of LIG-based MSCs capacitances from literature, using direct laser writing method.

Electrode	Design	Laser	Electrolyte	Capacitance	References
LIG/Borax-paper LIG/Borax-lignin-enriched paper LIG/Borax-cork	Sandwich	CO_2	PVA-H_2SO_4	(BP) 7.34 mF cm^{-2} (BLEP) 9.51 mF cm^{-2} (BC) 8.65 mF cm^{-2} @ 0.01 mA cm^{-1}	This work
LIG/Natural cork	Sandwich	UV	PVA-H_2SO_4	4.13 mF cm^{-2} @ 0.05 mA cm^{-2}	[18]
LIG/Kraft lignin	Sandwich	CO_2	PVA-H_2SO_4	2.51 mF cm^{-2} @ 0.01 mA cm^{-2}	[19]
LIG/Cork	Interdigitated	Fiber	PVA-H_2SO_4	1.43 mF cm^{-2} @ 0.1 mA cm^{-2}	[17]
LIG/Borax-paper	Interdigitated	CO_2	PVA-H_2SO_4	4.6 mF cm^{-2} @ 0.015 mA cm^{-2}	[21]
LIG/Polyimide	Interdigitated	CO_2	PVA-H_2SO_4	4 mF cm^{-2} @ 0.2 mA cm^{-2}	[46]
LIG/Polyimide	Sandwich	CO_2	PVA-H_2SO_4	9 mF cm^{-2} @ 0.02 mA cm^{-2}	[47]

A stability evaluation was conducted through 5000 cycles of charge–discharge (**Figure 7**) at a current density of 0.08 mA cm^{-2}.

During the cyclability test of all devices, it was observed that the paper-based MSCs demonstrated slightly better capacitance retention (≈85% of initial capacitance) compared to the cork MSCs (≈80% of initial capacitance). This capacitance loss of capacitance upon cycling is not ideal, but it is not uncommon. Some residual species resulting from the LIG processing are likely to exhibit irreversible reactions or poorly bound particles that degrade the capacitance during the first measurement cycles. Other authors also report that during the charge/discharge cycles of these devices, the observed loss of capacitance can be attributed to factors such as corrosion of electrode and substrate materials, decomposition of electrolyte water, and formation of gases in electrode pores, among others. Nevertheless, it is observed that after 3000 cycles, the MSCs capacitance tends to stabilize over time as expected, which is consistent with the literature.[17,21]

While the observed performance provides valuable insight into the potential applications of these devices, it is also crucial to also consider material stability and electrode-electrolyte interaction under demanding conditions over extended cycles. Compared to cork, paper substrates are typically thinner and more fragile, which may limit their suitability for prolonged use, particularly when using harsh electrolytes such as standard PVA-H_2SO_4, leading to substrate degradation over time. Nevertheless, BC MSCs demonstrate robustness and longevity, making them more suitable for energy storage applications in real-world scenarios, despite slightly lower capacitance retention compared to other materials. Further electrochemical characterization, namely Electrochemical impedance spectroscopy (EIC), can be found in the Supporting Information.

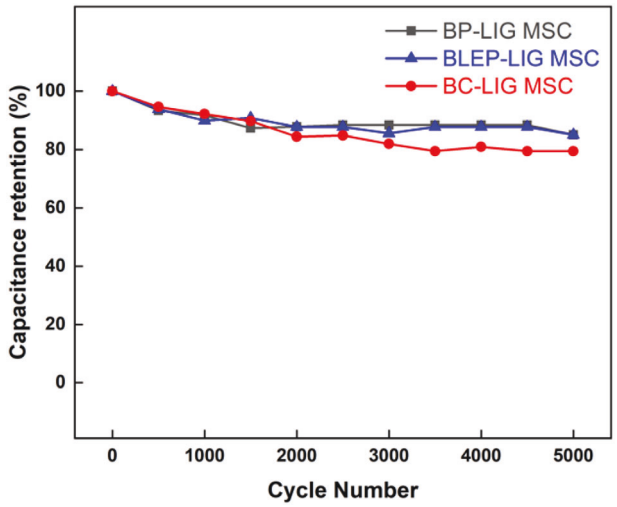

Figure 7. Comparison of the capacitance retention versus cycle number obtained from GCD curves of BP-LIG, BLEP-LIG, and BC-LIG MSC at a current density of 0.08 mA cm^{-2}.

2.4. Modular Assembly Characterization – Stacked and Sandwiched MSCs

To supply energy for practical applications, a single MSC is insufficient to power a system, so MSCs should be integrated into series or parallel configurations. This is essential to overcome the inherent limitations of the capacity of a single device. **Figure 8**a–c, GCD curves are presented, comparing a single device with two and three-stacked devices integrated into both series and parallel configurations. These experiments were conducted at a current density of 0.05 mA cm^{-2}.

The GCD curves reveal the expected behavior of EDL capacitors, characterized by a quasi-triangular shape and a slight *iR* drop across all devices.[48] Nonetheless, these curves show distinct performances among the different configurations and quantities of stacked devices.

Compared to a single device, the stacked series MSC demonstrates a cumulative voltage, featuring a 2× higher working voltage window (1.6 V) for two devices and a 3× higher working voltage window (2.4 V) for three devices, respectively. In contrast,

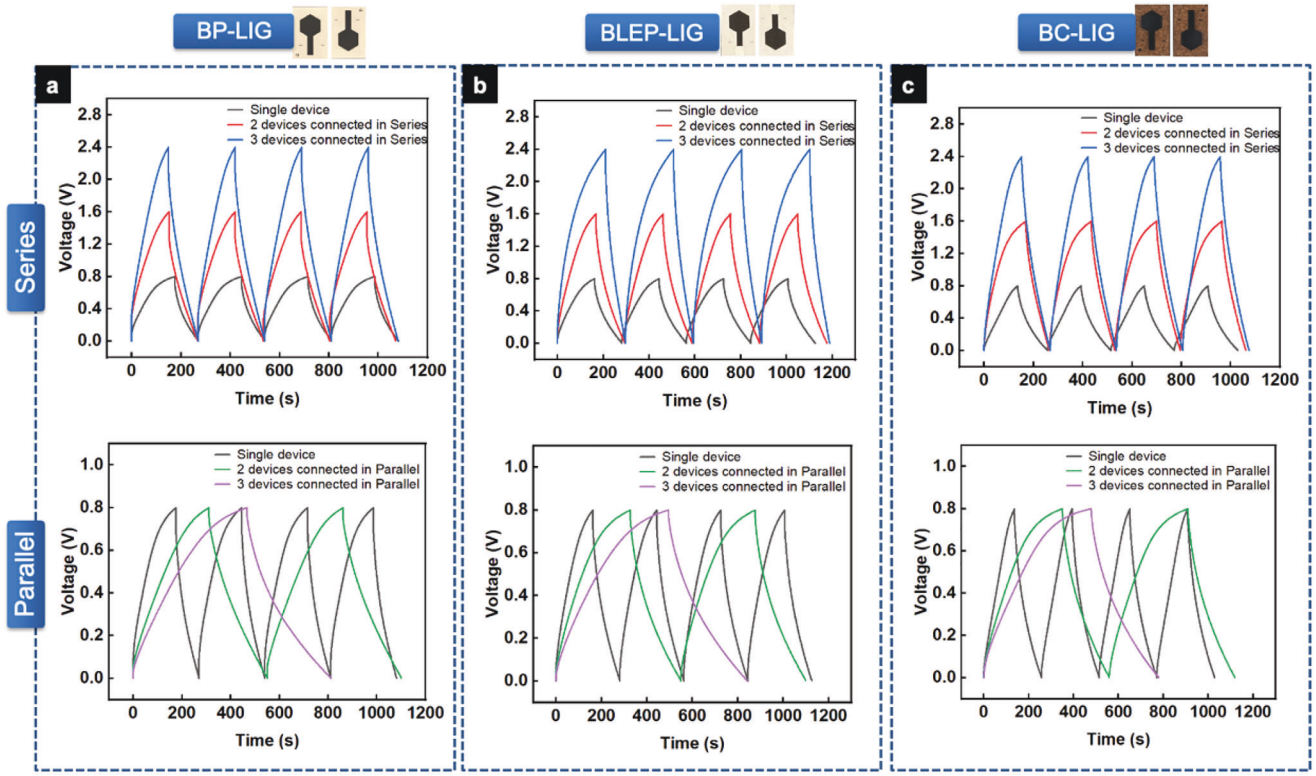

Figure 8. Electrochemical performances of single and stacked LIG-MSCs in series and parallel circuits. GCD curves comparing a single device to stacked series and parallel devices at a current density of 0.05 mA cm^{-2} in a) BP, b) BLEP, and c) BC based LIG MSCs.

the stacked parallel configuration exhibits a 2× longer discharge time for two devices and a 3× longer discharge time for three devices at the same current density. Consequently, this results in an enhanced overall capacitance achieved by adding MSCs. The extended discharge times emphasize the potential for increased energy storage capabilities, making parallel configurations favorable for applications requiring prolonged power delivery at lower voltage.[47] Moreover, the basic operational characteristics of both series and parallel connections are demonstrated by all MSCs, reinforcing the adaptability and feasibility of these configurations. Corresponding CV curves for stacked series and parallel MSCs can be found in Figure S4 (Supporting Information).

The versatility of integrating MSCs allows for tailored setups to meet specific application requirements, optimizing their performance for a diverse range of practical uses in electronic systems. As an example, and to validate their practicability, three BC MSCs were stacked in series, highly extending the voltage window from 0.8 to 2.4 V. A practical demonstration (**Figure 9**) shows that the assembled MSCs were able to successfully power both a multicolor light-emitting diode (LED) with a typical forward voltage in the range of 2–3.2 V and a humidity/temperature sensor with a forward voltage requirement of 1.5 V.

This demonstration not only proved the capability and simplicity of stacking and connecting multiple MSCs according to specific voltage requirements but also emphasized their potential across different applications. Videos demonstrating both examples can be found in the Supporting Information. The intermittent red, green, and blue (RGB) LED was powered for ≈30 s, while the humidity and temperature sensor were powered for roughly 3 min. The modular setup allows scalability, enabling the stacking of additional micro-supercapacitor units for increased energy storage and prolonged device operation. Moreover, these configurations have the potential to facilitate the development of energy-efficient, self-sustainable systems, particularly in low-power, low-resource, and remote sensing applications.

3. Conclusion

In summary, micro-supercapacitors were fabricated using green LIG electrodes were successfully fabricated on abundant, renewable, and non-toxic substrates, such as paper, lignin-enriched paper, and cork. The laser parameters were systematically optimized for each substrate, and a flame-retardant was incorporated to ensure efficient electrode production while preventing combustion and substrate ablation. Cork exhibited the lowest sheet resistance (≈10.6 ohm sq^{-1}), followed by lignin-enriched paper (≈45.5 ohm sq^{-1}) and paper (≈55.4 ohm sq^{-1}). This can be attributed to inherent material characteristics such as thermal resistance and lignin content.

The sustainable and stackable sandwich micro-supercapacitors demonstrated capacitance values of 7–10 mF cm^{-2}, which is consistent with prior research. The integration of these green LIG-based energy storage devices in various configurations offers potential for multifunctional platforms in renewable energy and off-grid technology. The study found out that cork is the preferred substrate material due to its natural

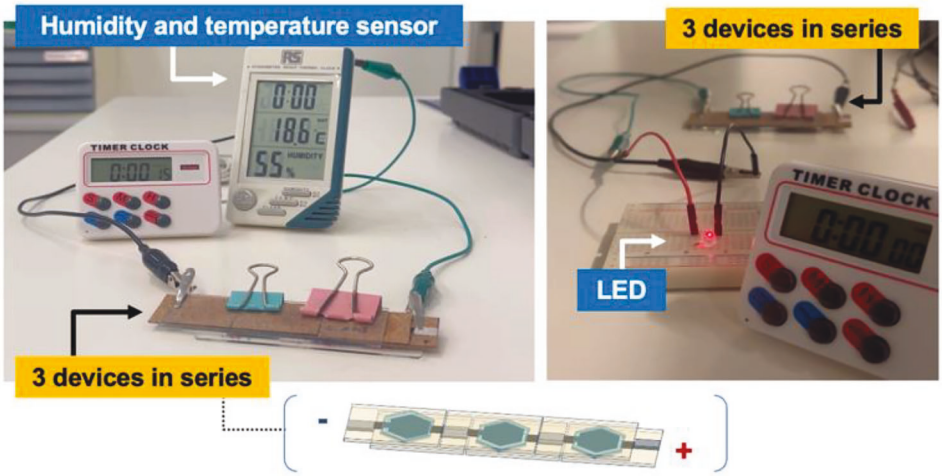

Figure 9. Humidity/temperature sensor and LED powered by three BC LIG-MSCs in series.

resilience and durability, making it well-suited for prolonged operational periods in demanding conditions. Practical demonstrations, such as powering an LED and a humidity/temperature sensor with a series of three BC MSC units, demonstrate the feasibility of this approach.

This methodology offers simplified and cost-effective means to achieve comparable or superior performance in electronic devices. It has the potential to further improve in laser graphitization efficiency, electrode geometries, and electrochemical properties, contributing to a more sustainable and technologically advanced future.

4. Experimental Section

Substrates Preparation and LIG Film Fabrication: Whatman paper 1 (Whatman International Ltd., Floram Park, NJ, USA), cork (Corticeira Amorim SGPS, S. A, Portugal), and lignin-enriched paper (provided by Eric Benson, E. Ainsley and Veronica Pham, University of Illinois, IL, USA) substrates were treated with borax, a flame-retardant agent, before undergoing laser irradiation. In a normal procedure, the substrates were soaked in an aqueous solution of sodium tetraborate decahydrate (0.1 M) ($Na_2B_4O_7{\cdot}10H_2O$; ≥99.5%; CAS: 1303-96-4) (Thermo Fisher Scientific, MA, USA) for 10 min and left to dry overnight. To ensure consistency, all substrates were leveled and lightly tapped on a glass surface before undergoing laser engraving. In the initial phase of the study, a preliminary investigation was conducted using a 75 W Epilog Fusion M2 CO_2 laser (10.6 µm wavelength – Epilog Laser, Golden, CO, USA), and under ambient conditions. LIG squares designed in CorelDraw, each measuring 5 mm × 5 mm, were submitted to the laser-controlling software and inscribed onto the treated substrates. This was achieved through the systematic variation of significant laser parameters, including a) power (adjustable up to 75 W), b) speed (adjustable up to 3.05 m s^{-1}), and c) defocus distance.

A frequency of 100 kHz and a resolution of 1200 dots-per-inch was maintained throughout all experiments. After optimizing all laser parameters, the optimal conditions for fabricating paper and lignin-enriched paper electrodes were obtained at a laser power of 4% and a speed of 13% (equivalent to 3 W @ 0.40 m s^{-1}). Similarly, for the cork substrate, optimal LIG electrode formation was achieved at a laser power of 4% and a speed of 6% (equivalent to 3 W @ 0.18 m s^{-1}). Additionally, positioning the laser beam 2 mm above the focal point for all substrates had been set as an optimal parameter.

LIG Characterization: The morphology and cross-sectional analysis of the produced LIG were analyzed using a Hitachi TM 3030Plus desktop workstation with Scanning Electron Microscopy. The X-ray Photoelectron Spectroscopy method with a Kratos Axis Supra instrument was used to analyze the chemical composition of the LIG substrates. The analysis utilized monochromatic Al Kα working at 150 W. Detailed scans were recorded with a 20 eV pass energy. For data analysis, CasaXPS software was used. Raman microscopy was performed using a Renishaw inViaTM Qontor confocal Raman microscope and a Renishaw Centrus 2957T3 detector. Excitation was carried out at 532 nm with a 10 mW green laser, focused via a 50× Olympus objective lens. For every measurement, three scans were undertaken, each with a 10-s exposure to a laser. Electrical characterization was carried out using a multimeter, followed by measuring the sheet resistance of LIG samples at room temperature using a BioRad HL5500 apparatus.

Design and Fabrication of Green Micro-Supercapacitors: The gLIG electrodes were laser-scribed onto borax-treated substrates with optimized lasing conditions. Hexagonal designs were created using Adobe Illustrator and laser patterned onto the substrates encompassing an area of 1 cm^2, using the optimized conditions. The current collector's conductor pads were coated with silver ink (silver-vinyl Cl-1001, Engineering Materials Systems, OH, USA), and then cured for 10 min at 90 °C. A PVA-H_2SO_4 aqueous gel was used as the solid electrolyte. A widely reported procedure was used to prepare the PVA-H_2SO_4 (1 M) electrolyte by dissolving PVA (1 g) (Thermo Fisher Scientific, MA, USA) in deionized water (10 mL) at 85 °C under gentle agitation. Then, 0.5 mL of sulfuric acid (Thermo Fisher Scientific, MA, USA) was added and left to stir vigorously for 1 h.[21] After cooling to room temperature, the PVA-H_2SO_4 solid electrolyte was cast onto the electrodes and subjected to a vacuum environment (≈−60 mPa) for 10 min to improve electrolyte penetration within the LIG matrix. Subsequently, MSC on sandwich configuration was assembled by carefully pressing the electrodes together with the electrolyte layer and a Whatman 1 paper separator in between. After assembling, the devices were left to dry overnight at room temperature, and then their electrochemical performance was assessed.

Electrochemical Characterization: The gLIG-based MSCs were connected to a PalmSens 4.0 Potentiostat/Galvanostat workstation (PalmSens Compact Electrochemical Interfaces, Netherlands) using silver pads under ambient conditions. Their electrochemical performance was evaluated through cyclic voltammetry conducted at various scan rates ranging from 5 to 100 mV s^{-1}, with a potential range of 0 to 0.8 V. Galvanostatic charge–discharge tests were performed on a CH Instruments Electrochemical Analyzer (CHI7081E model, CH Instruments, Inc., Austin, TX, USA) using current densities of 0.01, 0.02, 0.05, 0.1, and 0.2 mA cm^{-2}.

The potential window ranged from 0 to 0.8 V. Electrochemical impedance spectroscopy was carried out on a PalmSens 4.0 Potentiostat (PalmSens Compact Electrochemical Interfaces) using an AC voltage amplitude of 10 mV at the open circuit condition and a frequency range from 10 mHz to 1 MHz.

The areal capacitance, C_A, based on CV measurements, was calculated as follows[48]:

$$C_A = \frac{1}{2A\Delta Vs} \times \int (V)\, dV \quad (1)$$

where A denotes the total active area of the electrodes (with 1 cm^2 for the device produced in this work, ΔV represents the potential window (in V), s is the scan rate (in V s^{-1}) and $\int(V)dV$ is the integrated area of CV curve.

The areal capacitance, C_A, based on the charge–discharge profiles was calculated based on the equation:

$$C_A = \frac{I\Delta t}{A\Delta V} \quad (2)$$

where I represents the applied current, Δt is the discharge time, and A denotes the active area of the MSC. In this equation, $\Delta V = V_2 - V_1$, where V_2 is the potential at the beginning of discharge, post the internal resistance (IR) potential drop, while V_1 stands for the potential at the end of discharge. Energy (E_A) and power (P_A) densities per unit area were calculated as follows Equations (3) and (4):

$$E_A = \frac{1}{2} \frac{C_A \Delta V^2}{3600} \quad (3)$$

$$P_A = \frac{E_A}{\Delta t} \times 3600 \quad (4)$$

where, 3600 is the conversion factor transforming Watt-seconds (Ws) into Watt-hours (Wh). For a capacitance retention test, 5000 cycles were obtained from GCD curves at a current density of 0.08 mA cm^{-2}.

Data Analysis: Data analysis was performed using OriginPro (2022b Academic, MA, USA) for this study. Results are reported as mean ± standard deviation from at least three independent experiments, and the experimental design was a completely randomized study. All figures were also plotted in OriginPro (2022b Academic, MA, USA).

Supporting Information

Supporting Information is available from the Wiley Online Library or from the author.

Acknowledgements

This work was financed by national funds from the FCT—Fundação para a Ciência e a Tecnologia, I P, in the scope of the projects LA/P/0037/2020, UIDP/50025/2020, and UIDB/50025/2020 of the Associate Laboratory Institute of Nanostructures, Nanomodelling and Nanofabrication—i3N, and 2022.01493.PTDC (GAMBIT). This work was also partially supported by the European Union's Horizon Europe research and innovation program under grant agreement number 101096021 (SUPERIOT, HORIZON-JU-SNS-2022-STREAM-B-01-03). S.L.S. acknowledges PhD grant SFRH/BD/149751/2019. J.C. would like to acknowledge CEEC FCT/MCTES program (CEECIND/00880/2018) and EMERGIA Junta de Andalucía program (EMC21_00174). J.C. Claussen and C.L. Gomes would like to acknowledge funding support from the National Science Foundation under award number CMMI-202307026 (J.C.C.) and NSF PFI-TT-2141198 (J.C.C. and C.L.G). This study was supported by a Fulbright / FCT Research Grant, Portugal, AY 2022/2023. The authors thank Amorim Cork Composites for generously providing the cork samples, and to Eric Benson, E. Ainsley, and Veronica Pham from the University of Illinois for supplying the lignin-enriched paper samples used in this study.

Conflict of Interest

The authors declare no conflict of interest.

Author Contributions

S.L.S. performed conceptualization, methodology, wrote the original draft preparation, wrote the review and performed editing, formal analysis, and investigation. M.M., R.R.A.S., Z.T., and E.F. performed the review and editing. J.C.C. and C.L.G. performed validation, supervision, review and editing, and acquired funding. R.M. performed review and editing and acquired funding. L.P. performed validation, supervision, review and editing, and acquired funding. J.C. performed conceptualization, validation, supervision, wrote the review and performed editing, and acquired funding. The manuscript was written through contributions of all authors. All authors have given approval to the final version of the manuscript.

Data Availability Statement

The data that support the findings of this study are available in the supplementary material of this article.

Keywords

cellulose-based substrates, direct laser writing, green electronics, supercapacitors, sustainability

Received: February 15, 2024
Revised: April 24, 2024
Published online: May 16, 2024

[1] S. Weiland, T. Hickmann, M. Lederer, J. Marquardt, S. Schwindenhammer, *Polit. Govern.* **2021**, *9*, 1.
[2] W. Li, Q. Liu, Y. Zhang, C. Li, Z. He, W. C. H. Choy, P. J. Low, P. Sonar, A. K. K. Kyaw, *Adv. Mater.* **2020**, *32*, 2001591.
[3] C. P. Baldé, R. Kuehr, T. Yamamoto, R. McDonald, S. Althaf, G. Bel, O. Deubzer, E. Fernandez-Cubillo, V. Forti, V. Gray, S. Herat, S. Honda, G. Iattoni, D. S. Khetriwal, V. L. d. Cortemiglia, *International Telecomunication Union (ITU) and United Nations Institute for Training and Research (UNITAR)*, https://www.itu.int/itu-d/sites/environment (accessed: April 2004).
[4] J. A. P. Silva, G. G. Lima, C. F. Camilo-Cotrim, E. F. L. C. Bailão, S. S. Caramori, J. C. Nabout, L. M. Almeida, *Water Air Soil Pollut.* **2023**, *234*, 320.
[5] Z. Hui, L. Zhang, G. Ren, G. Sun, H. Yu, W. Huang, *Adv. Mater.* **2023**, *35*, 2211202.
[6] H. Zhu, W. Luo, P. N. Ciesielski, Z. Fang, J. Y. Zhu, G. Henriksson, M. E. Himmel, L. Hu, *Chem. Rev.* **2016**, *116*, 12650.
[7] Y. Xu, Q. Fei, M. Page, G. Zhao, Y. Ling, S. B. Stoll, Z. Yan, *iScience* **2021**, *24*, 102736.
[8] S. M. Khan, J. M. Nassar, M. M. Hussain, *ACS Appl. Electron. Mater.* **2021**, *3*, 30.
[9] C. Santato, P. Alarco, *Adv. Mater. Technol.* **2022**, *7*, 2101265.
[10] T. D. Le, H. Phan, S. Kwon, S. Park, Y. Jung, J. Min, B. J. Chun, H. Yoon, S. H. Ko, S. Kim, Y. Kim, *Adv. Funct. Mater.* **2022**, *32*, 2205158.
[11] P. I. C. Claro, T. Pinheiro, S. L. Silvestre, A. C. Marques, J. Coelho, J. M. Marconcini, E. Fortunato, L. H. C. Mattoso, R. Martins, *Appl. Phys. Rev.* **2022**, *9*, 041305.
[12] T. D. Le, S. Park, J. An, P. S. Lee, Y. Kim, *Adv. Funct. Mater.* **2019**, *29*, 1902771.

[13] A. C. Bressi, A. Dallinger, Y. Steksova, F. Greco, *ACS Appl. Mater. Interfaces* **2023**, *15*, 35788.
[14] T. Pinheiro, S. Silvestre, J. Coelho, A. C. Marques, R. Martins, M. G. F. Sales, E. Fortunato, *Adv. Mater. Interfaces* **2021**, *8*, 2101502.
[15] L. F. Mendes, A. de Siervo, W. Reis de Araujo, T. R. Longo Cesar Paixão, *Carbon* **2020**, *159*, 110.
[16] G. Cantarella, M. Madagalam, I. Merino, C. Ebner, M. Ciocca, A. Polo, P. Ibba, P. Bettotti, A. Mukhtar, B. Shkodra, A. S. Inam, A. J. Johnson, A. Pouryazdan, M. Paganini, R. Tiziani, T. Mimmo, S. Cesco, N. Münzenrieder, L. Petti, N. Cohen, P. Lugli, *Adv. Funct. Mater.* **2023**, *33*, 2210422.
[17] S. L. Silvestre, T. Pinheiro, A. C. Marques, J. Deuermeier, J. Coelho, R. Martins, L. Pereira, E. Fortunato, *Flex. Print. Electronics* **2022**, *7*, 035021.
[18] A. Imbrogno, J. Islam, C. Santillo, R. Castaldo, L. Sygellou, C. Larrigy, R. Murray, E. Vaughan, M. d. K. Hoque, A. J. Quinn, D. Iacopino, *ACS Appl. Electron Mater.* **2022**, *4*, 1541.
[19] F. Mahmood, H. Zhang, J. Lin, C. Wan, *ACS Omega* **2020**, *5*, 14611.
[20] Y. Tan, Y. Ren, Z. Xu, Y. Zhu, H. Li, *J. Electron. Mater.* **2023**, *52*, 2603.
[21] J. Coelho, R. F. Correia, S. Silvestre, T. Pinheiro, A. C. Marques, M. R. P. Correia, J. V. Pinto, E. Fortunato, R. Martins, *Microchimica Acta* **2023**, *190*, 40.
[22] R. Miyakoshi, S. Hayashi, M. Terakawa, *RSC Adv.* **2022**, *12*, 29647.
[23] B. Kulyk, B. F. R. Silva, A. F. Carvalho, P. Barbosa, A. V. Girão, J. Deuermeier, A. J. S. Fernandes, F. M. L. Figueiredo, E. Fortunato, F. M. Costa, *Adv. Mater. Technol.* **2022**, *7*, 2101311.
[24] A. F. Carvalho, A. J. S. Fernandes, R. Martins, E. Fortunato, F. M. Costa, *Adv. Mater. Technol.* **2020**, *5*, 2000630.
[25] B. Kulyk, B. F. R. Silva, A. F. Carvalho, S. Silvestre, A. J. S. Fernandes, R. Martins, E. Fortunato, F. M. Costa, *ACS Appl. Mater. Interfaces* **2021**, *13*, 10210.
[26] R. Zhang, B. Wang, T. Xiao, M. Wang, Z. Wu, X. Xiao, *Mater. Sci. Energy Technol.* **2023**, *6*, 547.
[27] A. Velasco, Y. K. Ryu, A. Boscá, A. Ladrón-de-Guevara, E. Hunt, J. Zuo, J. Pedrós, F. Calle, J. Martinez, *Sustainable Energy Fuels* **2021**, *5*, 1235.
[28] M. Wang, J. Chen, K. Lu, Y. Ma, H. Li, J. Ye, *Electrochim. Acta* **2022**, *401*, 139490.
[29] R. Ye, Y. Chyan, J. Zhang, Y. Li, X. Han, C. Kittrell, J. M. Tour, *Adv. Mater.* **2017**, *29*, 1702211.
[30] G. Yuan, T. Wan, A. BaQais, Y. Mu, D. Cui, M. A. Amin, X. Li, B. Bin Xu, X. Zhu, H. Algadi, H. Li, P. Wasnik, N. Lu, Z. Guo, H. Wei, B. Cheng, *Carbon* **2023**, *212*, 118101.
[31] Z. Peng, R. Ye, J. A. Mann, D. Zakhidov, Y. Li, P. R. Smalley, J. Lin, J. M. Tour, *ACS Nano* **2015**, *9*, 5868.
[32] M. Khandelwal, C. V. Tran, J. Lee, J. Bin In, *Chem. Eng. J.* **2022**, *428*, 131119.
[33] A. Velasco, Y. K. Ryu, A. Hamada, A. de Andrés, F. Calle, J. Martinez, *Nanomaterials* **2023**, *13*, 788.
[34] W. Ma, J. Zhu, Z. Wang, W. Song, G. Cao, *Mater Today Energy* **2020**, *18*, 100569.
[35] R. Ye, D. K. James, J. M. Tour, *Adv. Mater.* **2019**, *31*, 1803621.
[36] Y. Chyan, R. Ye, Y. Li, S. P. Singh, C. J. Arnusch, J. M. Tour, *ACS Nano* **2018**, *12*, 2176.
[37] O. Castro, J. M. Silva, T. Devezas, A. Silva, L. Gil, *Mater. Des.* **2010**, *31*, 425.
[38] G. Dombek, Z. Nadolny, P. Przybylek, R. Lopatkiewicz, A. Marcinkowska, L. Druzynski, T. Boczar, A. Tomczewski, *Energies* **2020**, *13*, 4433.
[39] F. M. Vivaldi, A. Dallinger, A. Bonini, N. Poma, L. Sembranti, D. Biagini, P. Salvo, F. Greco, F. Di Francesco, *ACS Appl. Mater. Interfaces* **2021**, *13*, 30245.
[40] M. G. Stanford, C. Zhang, J. D. Fowlkes, A. Hoffman, I. N. Ivanov, P. D. Rack, J. M. Tour, *ACS Appl. Mater. Interfaces* **2020**, *12*, 10902.
[41] W. Qu, Z. Zhao, J. Wang, F. Dong, H. Xu, X. Sun, H. Jin, *Sustain. Energy Fuels* **2021**, *5*, 3744.
[42] M. Wall, *Therm. Scientif.* **2011**, *5*.
[43] H. Liu, G. Zhang, X. Zheng, F. Chen, H. Duan, *Int. J. Extrem. Manufact.* **2020**, *2*, 042001.
[44] K. Lee, S. Kim, M. Kim, D. B. Ahn, Y. Hong, S. Kim, J. S. Lee, S. Lee, *Adv. Energy Mater.* **2023**, *13*, 2204327.
[45] J. Huang, Y. Xie, Y. You, J. Yuan, Q. Xu, H. Xie, Y. Chen, *Adv. Funct. Mater.* **2023**, *33*, 2213095.
[46] J. Lin, Z. Peng, Y. Liu, F. Ruiz-Zepeda, R. Ye, E. L. G. Samuel, M. J. Yacaman, B. I. Yakobson, J. M. Tour, *Nat. Commun.* **2014**, *5*, 5714.
[47] Z. Peng, J. Lin, R. Ye, E. L. G. Samuel, J. M. Tour, *ACS Appl. Mater. Interfaces* **2015**, *7*, 3414.
[48] *Supercapacitors: Materials, Systems, And Applications*, Wiley, Hoboken, New Jersey, USA **2013**, https://onlinelibrary.wiley.com/doi/book/10.1002/9783527646661.